ISSN 0036-0236, Russian Journal of Inorganic Chemistry, 2009, Vol. 54, No. 12, pp. 1857–1861. © Pleiades Publishing, Inc., 2009.
Original Russian Text © V.K. Ivanov, G.P. Kopitsa, A.E. Baranchikov, S.V. Grigor'ev, V.V. Runov, V. Garamus, 2009, published in Zhurnal Neorganicheskoi Khimii, 2009, Vol. 54, No. 12, pp. 1939–1943.

SYNTHESIS AND PROPERTIES OF INORGANIC COMPOUNDS

Hydrothermal Growth of Ceria Nanoparticles

V. K. Ivanov[a], G. P. Kopitsa[b], A. E. Baranchikov[a], S. V. Grigor'ev[b], V. V. Runov[b], and V. M. Haramus[c]

[a] *Kurnakov Institute of General and Inorganic Chemistry, Russian Academy of Sciences, Leninskii pr. 31, Moscow, 119991 Russia*

[b] *Konstantinov Institute of Nuclear Physics, Russian Academy of Sciences, Gatchina, Leningrad oblast, 188300 Russia*

[d] *GKSS Research Centre, Geesthacht, Germany*

Received December 23, 2008

Abstract—Peculiarities of CeO_2 nanoparticle coarsening during hydrothermal treatment in a neutral medium are determined by small-angle neutron scattering, powder X-ray diffraction, low-temperature nitrogen adsorption, and transmission electron microscopy. Coherent intergrowth of individual CeO_2 crystallites is the main scenario of nanoparticle coarsening.

DOI: 10.1134/S0036023609120018

One popular way to prepare oxide powders during the last decades is hydrothermal synthesis, which accomplishes chemical reactions in aqueous solution at temperatures above 100°C and pressures above 1 atm. Varying hydrothermal treatment parameters, including the temperature schedule and duration, concentration and acidity (pH) of solutions treated, and system's pressure, offer a means for synthesizing a wide range of inorganic materials with the desired micromorphology and structure-sensitive properties [1].

The first works on the hydrothermal synthesis of ultrafine and nanodisperse ceria powders were published in the early 1980s–1990s [2, 3]. Tani et al. [2] showed that increasing treatment temperature and duration or adding mineralizers (KF, LiCl, LiBr, K_2CO_3, $LiNO_3$, Li_2SO_4, and NaOH) is useful to enhance ceria particle growth.

Hirano and Kato [4, 5] were the first to systematically study the effect of the hydrothermal treatment temperature (within 120–200°C) and time (5–40 h) on ceria particle sizes. They showed that the hydrothermal treatment of slurries having the nitrate history for 5 h at temperatures up to 180°C does not alter CeO_2 crystallite sizes (~2 nm). When cerium(IV) sulfate is used as the precursor, the particle size depends on both the synthesis parameters (time and temperature) and the solution concentration.

Lakhwani and Rahaman [6] also studied the effect of hydrothermal treatment parameters on the CeO_2 particle coarsening dynamics. They found that the CeO_2 particle growth kinetics obey the parabolic law; in their opinion, this indicates that particle coarsening during hydrothermal treatment follows the Ostwald ripening model according to the Lifshits–Slyozov–Wagner distribution. However, they found the CeO_2 particle growth rates to differ considerably depending on whether samples had a chloride or nitrate history; the CeO_2 particle sizes synthesized from cerium(III) nitrate ranged from 9 to 20 nm, whereas the CeO_2 particles synthesized from cerium(III) chloride had their sizes virtually unchanged (13.5–15.5 nm). Lakhwani and Rahaman [6] do not specify the reasons for these distinctions, but their results are at variance to the dissolution/crystallization model they use, because in this case the CeO_2 nanoparticle growth dynamics should be controlled by particle size solely, rather than by their history.

Presumably, the aforementioned distinctions arise from the fact that, actually, hydrothermal growth of CeO_2 nanoparticles can obey the oriented crystallite attachment scenario, which was first described by Penn and Banfield [7]. The essence of this phenomenon is as follows: when two or more crystalline nanoparticles collide in a liquid medium and stick together, they can rotate so that their faces with identical crystallographic indices are parallel to each other, followed by coherent intergrowth of nanoparticles to form single-crystal particles or polycrystals separated by twin boundaries or other planar defects. Another argument in favor of the above suggestion is provided by the extremely low water solubility of ceria in the absence of mineralizers [8], which makes unlikely CeO_2 particle growth by the dissolution/crystallization mechanism.

Therefore, this work studies CeO_2 particle size variation trends during hydrothermal treatment (120–210°C) in a neutral medium and determines the major particle growth mechanism.

EXPERIMENTAL

The precursor nanodisperse ceria was prepared as described in [9]. A vigorously stirred solution of

cerium(III) nitrate (0.08 mol/L) in water/isopropanol (1 : 1) was rapidly added to aqueous ammonia (3 mol/L) taken in a fivefold molar excess and allowed to stand for 3 h at room temperature. A precipitate was carefully washed with distilled water until the mother solution acquired neutral pH, centrifuged at 8 000 rpm, and dried for 24 h at 60°C.

Microwave-hydrothermal (MW-HT) treatment of ceria slurries in distilled water was carried out on a Berghof Speedwave MWS-3+ setup for 3 h at 120, 150, 180, and 210°C and for 15 min at 120 and 210°C. 100-mL polytetrafluoroethylene autoclaves were used; their fillage was 50%. The slurry temperature was monitored using an IR pyrometer (at 150°C the temperature determination error was ±1 K). After an experiment was over, autoclaves were taken from the furnace and cooled to room temperature. Products were recovered by centrifugation, repeatedly washed with distilled water, and dried for 2 h in air at 60°C.

Powder X-ray diffraction analysis was carried out on a Rigaku D/MAX 2500 diffractometer (CuK_α radiation); the goniometer rotation speed was 2°2θ/min. Diffraction peaks were identified with reference to the JCPDS database. Coherent scattering lengths for ceria samples were determined from the Scherrer relationship

$$D_{hkl} = \frac{K\lambda}{\beta_{hkl}(2\theta)\cos(\theta_0)}, \quad (1)$$

where θ_0 is the peak position; λ is the CuK_α radiation wavelength, equal to 0.154056 nm; and $\beta_{hkl}(2\theta)$ is the true physical broadening of the diffraction peak. The Scherrer constant (K) was set equal to unity.

The physical broadening was calculated from

$$\beta_{hkl} = \beta - s, \quad (2)$$

where β is the full width at half-height of the X-ray diffraction peak and s is the instrumental broadening (0.09° ± 0.01°2θ). The contribution from microstresses to peak broadening was ignored. A sapphire single crystal was used as a reference to apply correction for instrumental broadening.

The β value was calculated after subtraction background using the pseudo-Voigt function fit of the (111) and (200) peak profiles within 20°–40°2θ:

$$V(\theta) = \frac{2cA}{\pi}\left[\frac{\omega_L}{4(\theta-\theta_0)^2+\omega_L^2}\right] + \frac{2(1-c)A}{\omega_G}\sqrt{\frac{\ln 2}{\pi}}\exp\left[-\frac{4\ln 2(\theta-\theta_0)^2}{\omega_G^2}\right], \quad (3)$$

Here, ω_L and ω_G are, respectively, the Lorentzian and Gaussian parameters ($\omega_L = \omega_G = \beta$), A is the scaling factor, and c is the relative contribution of the Lorentz function to the overall reflection intensity.

The D_{hkl} values calculated from $\beta_{111}(2\theta)$ and $\beta_{200}(2\theta)$ differed by no more than 0.2 nm. The arithmetic mean between D_{111} and D_{200} was used as the coherent scattering length (crystallite size).

The Rietveld refinement of the unit cell parameters for ceria samples was carried out using JANA2000 software [10]. Peak profiles were fitted to pseudo-Voigt functions in the range 15°–90°2θ including the nonmonochromaticity of CuK_{α_1} and CuK_{α_2} radiations. Background lines were fitted to 15th-order Chebyshev polynomials.

Microstructure was observed using transmission electron microscopy (TEM) on a Leo912 AB Omega electron microscope at an accelerating voltage of 100 kV (magnification ×500000).

Specific surface areas of CeO_2 powders were measured by low-temperature nitrogen adsorption using an ATX-06 analyzer. The carrier gas was helium (type A). Before measurements, test samples were degassed for 30 min at 150°C in air. The nitrogen partial pressure was determined using a katharometer whose temperature was adjusted to 45.00°C. The instrument was calibrated before measurements to improve the pressure determination accuracy. The results of the measurements were used to calculate the eight-point Brunauer–Emmet–Teller (BET) specific surface area

Small-angle neutron scattering (SANS) was measured on a SANS-1 setup (FRG1 reactor, GKSS Research Centre, Geesthacht, Germany) at the neutron wavelength λ = 8.19 Å ($\Delta\lambda/\lambda$ = 10%) at four sample–detector distances (SD = 0.7, 1.8, 4.5, and 9 m), which allowed neutron scattering intensities to be measured in the range of momentum transfer $4.5 \times 10^{-3} < q < 2.5 \times 10^{-1}$ Å^{-1}. Scattered neutrons were detected by a ^{3}He position-sensitive area detector.

CeO_2 nanopowder samples were placed to quartz glass cells 1 mm thick. Initial spectra for each q range were corrected for the scattering from the setup hardware, cell, and ambience using a standard procedure [11]. The thus-obtained two-dimensional isotropic spectra were azimuthally averaged and reduced to absolute magnitudes via scaling to the vanadium incoherent scattering cross section with account for the detector efficiency [11] and bulk density ρ_b for each sample. All measurements were carried out at room temperature.

The SANS intensity $I_s(q)$ was determined in this work as

$$I_s(q) = I(q) - TI_0(q), \quad (4)$$

Here, $I(q)$ and $I_0(q)$ are the q distributions of scattering neutrons behind the sample and the beam without sample, respectively; and T is the transmission coefficient for transmitted neutrons:

$$T = I/I_0 = e^{(-\Sigma L)}, \quad (5)$$

where $\Sigma = \sigma_s + \sigma_a$ is the integral cross section, including the nuclear scattering σ_s and absorption σ_a, and L is the sample thickness.

The SANSFIT program [12] was used to transform SANS curves to particle-size distribution functions.

RESULTS AND DISCUSSION

Powder X-ray diffraction demonstrates that the MW-HT treatment of CeO_2 slurry samples having a nitrate history at 120–180°C does not increase the crystallite sizes (D_{CSL} = 5 nm) in good agreement with the Hirano and Kato results [4, 5]. An insignificant increase in D_{CSL} (to 6 nm) is observed only when the treatment temperature and duration increase to 210°C and 3 h, respectively (table). The specified trend is verified by the analysis of the CeO_2 init cell parameter. The table shows a noticeable decrease in the unit cell parameter indicating CeO_2 nanoparticle coarsening [13] only for sample Ce-210-180.

Low-temperature nitrogen adsorption indicates that the specific surface area of ceria nanopowders is virtually unaffected by the MW-HT treatment parameters and reaches 130–150 m^2/g.

Small-angle neutron scattering was used to highlight more structural features of ceria samples, and Figure 1 displays representative log–log plots of scattering cross sections $d\Sigma(q)/d\Omega$ for the as-synthesized CeO_2 sample obtained and for samples experienced MW-HT treatment at 210°C for 15 min and 3 h.

The examination of the SANS curves is useful for the restoration of the size distribution function for scattering inhomogeneities (particles):

$$D_V(R) = D_N(R)V, \quad (6)$$

Here, $D_N(R)$ is particle-radius distribution density function and V is particle volume. We used an indirect Fourier transformation [12, 14] for estimating the $D_V(R)$ function; this transformation is less sensitive to a break at small radii that occurs in real systems. Figure 2 displays the resulting particle-size distribution functions $D_V(R)$ for samples synthesized using various MW-HT treatment temperatures and durations.

The above data imply that all CeO_2 sampl tested are characterized by a bimodal particle size distribution. The second peak position corresponds to a doubled particle size for the first distribution peak.

Noteworthy, the MW-HT treatment of the as-synthesized ceria sample at 120°C for 15 min or 3 h does not considerably change particle-size distributions (Fig. 2a). The 15-min treatment at 210°C increases the volume fraction of larger particles but decreases the fraction of fine particles corresponding to the first distribution peak (Fig. 2b). Increasing MW-HT treatment duration at this temperature to 3 h enhances the decrease in the first peak height and the proportional increase in the second distribution peak height (Fig. 2c).

Crystallite sizes and unit cell parameters for ceria samples prepared by MW-HT treatment

Sample notation	MW-HT treatment temperature and duration	D_{111}, nm	D_{200}, nm	a, Å
Ce-1 (untreated sample)	–	5.0	4.8	5.4235
Ce-120-15	120°C, 15 min	5.0	4.9	5.4208
Ce-120-180	120°C, 180 min	5.0	4.9	5.4209
Ce-150-180	150°C, 180 min	5.1	5.0	5.4210
Ce-180-180	180°C, 180 min	5.2	5.1	5.4203
Ce-210-15	210°C, 15 min	5.2	5.0	5.4188
Ce-210-180	210°C, 180 min	6.1	5.9	5.4123

The aforementioned evolution of the CeO_2 powder micromorphology in response to increasing hydrothermal treatment temperature and duration cannot be interpreted in terms of the Ostwald ripening model (in particular, the dissolution–crystallization scenario). Indeed, if particles were grown by this scenario, the particle size distribution peak would have shifted toward larger sizes, which is actually not observed in the case at hand. At the same time, the trends of the particle size distribution curves are well fitted by the oriented attachment particle growth model. The following arguments are in favor of this model: (a) the constancy of the first distribution peak position, (b) the specifics of the mutual arrangement of the first and second distribution peaks (particle size doubling), and (c) the change in relative contributions from the first and sec-

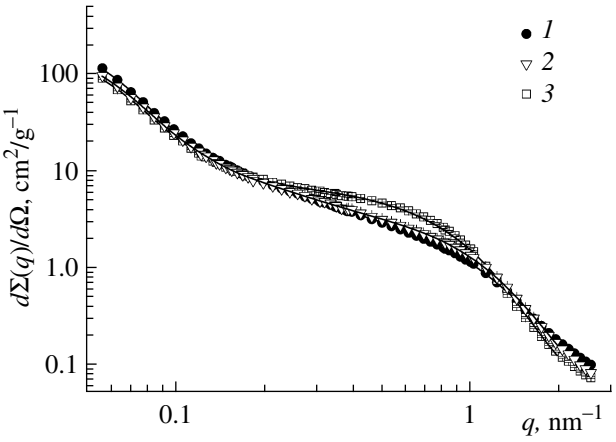

Fig. 1. SANS cross section $d\Sigma(q)/d\Omega$ vs. momentum transfer q for samples (*1*) Ce-1, (*2*) Ce-210-15, and (*3*) Ce-210-180.

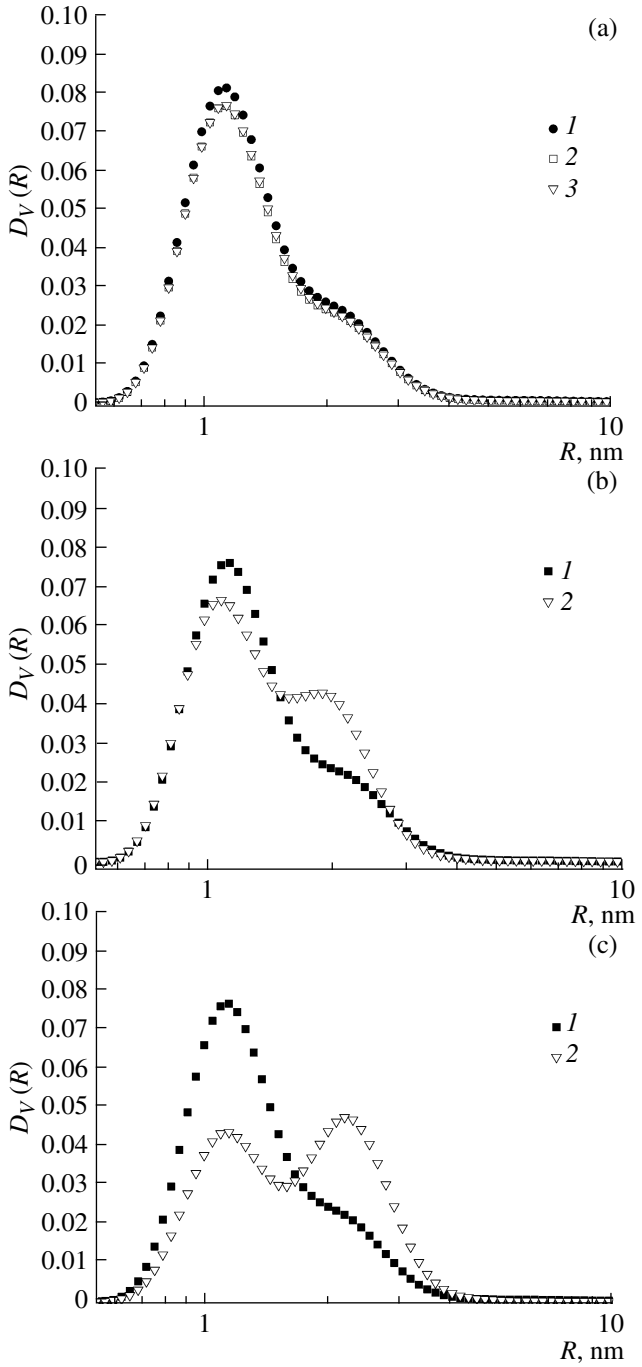

Fig. 2. Particle size distribution functions $D_V(R)$ for samples synthesized by MW-HT treatment with various temperatures and durations. Panel (a): samples (*1*) Ce-1, (*2*) Ce-120-15, and (*3*) Ce-120-180. Panel (b): samples (*1*) Ce-120-15 and (*2*) Ce-210-15. Panel (c): samples Ce-120-180 and (*2*) Ce-210-180.

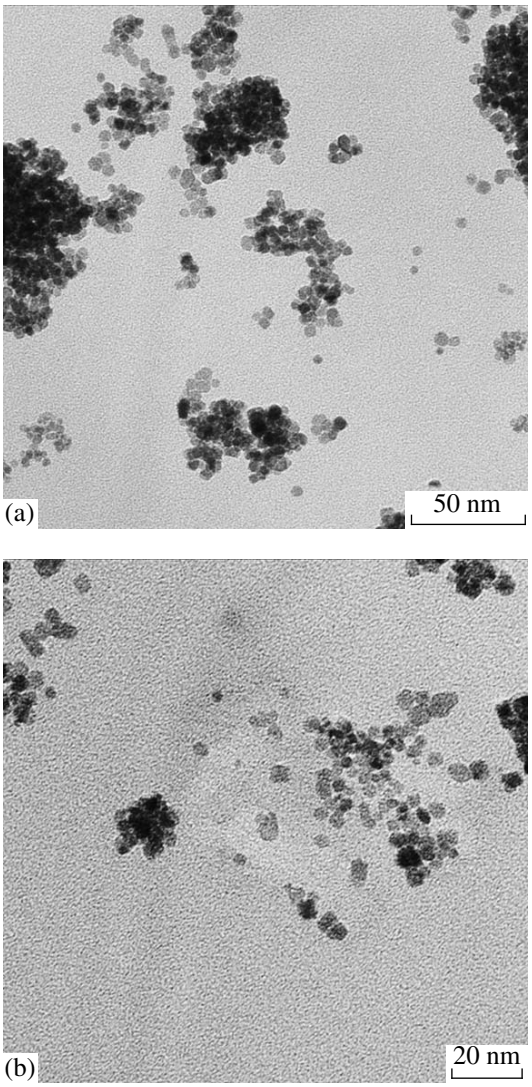

Fig. 3. Micrographs of sample Ce-210-180.

ond distribution peaks caused by increasing MW-HT treatment temperature and duration.

Ceria micrographs verify the above inferences made from SANS data. TEM micrographs show that CeO_2 particles can be mutually oriented relative to one another to form plane-parallel boundaries (Fig. 3a) and grow together to form elongated irregularly shaped particles (Fig. 3b). Noteworthy, anisotropic ceria particles cannot form by the dissolution/crystallization scenario, because this compound crystallizes in cubic system.

In summary, we have studied for the first time the specifics of ceria nanoparticle coarsening during microwave-hydrothermal treatment using a set of analytical methods. We have shown that the oriented attachment of individual CeO_2 crystallites is the main scenario of CeO_2 particle coarsening.

ACKNOWLEDGMENTS

This work was supported by the Russian Foundation for Basic Research (project no. 08-03-00471) and Program no. 27 of the Russian Academy of Sciences "Fundamentals of Basic Research into Nanotechnologies

and Nanomaterials." The Russian authors appreciate the hospitality of the GKSS Research Centre.

REFERENCES

1. *Handbook of Hydrothermal Technology* (William Andrew, New York, 2001).
2. E. Tani, M. Yoshimura, and S. Somiya, J. Mater. Sci. Lett. **1**, 461 (1982).
3. Y. C. Zhou and M. N. Rahaman, J. Mater. Res. **8**, 1680 (1993).
4. M. Hirano and E. Kato, J. Am. Ceram. Soc. **79**, 777 (1996).
5. M. Hirano and E. Kato, J. Mater. Sci. Lett. **15**, 1249 (1996).
6. S. Lakhwani and M. N. Rahaman, J. Mater. Res. **14**, 1455 (1999).
7. R. L. Penn and J. F. Banfield, Science **281**, 969 (1998).
8. M. Takaya, Y. Shinohara, F. Serita, et al., Ind. Health **44**, 639 (2006).
9. V. K. Ivanov, O. S. Polezhaeva, G. P. Kopitsa, et al., Neorg. Mater. **44**, 272 (2008).
10. V. Petricek, M. Dusek, and L. Palatinus, *Jana 2006. The Crystallographic Computing System* (Inst. of Physics, Prague, 2006).
11. G. D. Wignall and F. S. Bates, J. Appl. Crystallogr. **20**, 28 (1986).
12. P. Biemann, M. Haese-Seiller, and P. Staron, Physica B **276—278**, 156 (2000).
13. F. Zhang, S.-W. Chan, J. E. Spanier, et al., Appl. Phys. Lett. **80**, 127 (2002).
14. D. I. Svergun and L. A. Feigin, *X-ray and Neutron Small-Angle Scattering* (Nauka, Moscow, 1986) [in Russian].